# FABRICATION AND CHARACTERIZATION OF DENSE CERAMIC MEMBRANES FOR PARTIAL OXIDATION OF METHANE*

U. Balachandran, B. Ma, J. T. Dusek, J. J. Picciolo,
R. L. Mieville, and P. S. Maiya
Energy Technology Division
Argonne National Laboratory
Argonne, IL 60439

and

M. S. Kleefisch and C. A. Udovich
Amoco Research Center
Naperville, IL 60566

June 1995



For presentation at the Coal Liquefaction and Gas Conversion Contractors' Review Conference, August 29–31, 1995, Pittsburgh, PA.

*Work at Argonne National Laboratory is supported by the U.S. Department of Energy, Pittsburgh Energy Technology Center, under Contract W-31-109-Eng-38.

# FABRICATION AND CHARACTERIZATION OF DENSE CERAMIC MEMBRANES FOR PARTIAL OXIDATION OF METHANE

U. Balachandran, B. Ma, J. T. Dusek, J. J. Picciolo,
R. L. Mieville, and P. S. Maiya
Energy Technology Division
Argonne National Laboratory
Argonne, IL 60439

and

M. S. Kleefisch and C. A. Udovich
Amoco Research Center
Naperville, IL 60566

## INTRODUCTION

A significant reduction in the cost of syngas would have a major effect on the future direction of fuel and chemical production. Syngas production accounts for up to 60–70% of the total cost of most integrated systems that produce chemical and hydrocarbon liquids. Syngas is also a major source of hydrogen, which is in ever-increasing demand for the removal of pollutants from fossil fuels.

A recent innovation [1,2] that could bring down the production cost of syngas is the use of ceramic membranes in a partial oxidation mode or in a combined mode of partial oxidation and steam reforming. In this review, we offer a technology that is based on dense ceramic membranes and that uses air as the oxidant for methane conversion reactions, thus eliminating the need for an expensive oxygen plant. Oxygen separation plants are the single most costly item in the production of syngas by partial oxidation.

Certain ceramic materials exhibit both electronic and ionic conductivities (of particular interest is oxygen-ion conductivity). These materials transport not only oxygen ions (functioning as selective oxygen separators) but also electrons back from the reactor side to the oxygen/reduction interface. No external electrodes are required and if the driving potential of transport is sufficient, the partial-oxidation reactions should be spontaneous. Such a system will operate without an externally applied potential. Oxygen is transported across the ceramic material in the form of oxygen anions, not oxygen molecules.

Recent reports in the literature suggest that dense ceramic membranes made of these mixed conductors can successfully separate oxygen from air at flux rates that could be considered commercially feasible, and thus can have the potential to improve the economics of methane conversion processes [1-11].

One such class of mixed conductors is the perovskites, which are oxides based on the structure of the cubic-lattice mineral perovskite, $CaTiO_3$ [12]. Partial substitution of a higher-valency cation (donor-dopant) for a lower metal ion results in two types of charge compensation, namely, electronic and ionic, depending on the partial pressure of oxygen in equilibrium with the oxides [13,14]. The charge compensation in acceptor-doped oxides (i.e., substituting a divalent cation for a trivalent cation) is by electronic holes at high oxygen pressures, but by oxygen-ion vacancies at low pressures [10,15]. Ion vacancies are the pathways for oxide ions; therefore, oxygen flux can be increased by increasing the amount of acceptor-dopant. Reported oxygen flux values [1-3,10,11] for perovskites tend to follow the trends suggested by the charge compensation theory. Although not all of the mixed oxides we have made are perovskites, the suggested mechanism outlined above is believed to hold true for other similar oxides.

## EXPERIMENTAL

Several LaSrFeCo mixed oxides (designated as SFC) of different stoichiometries (see Table 1) are made by solid-state reaction of the constituent cationic salts. Most of the performance evaluation has concentrated on SFC-2, a nonperovskite mixed oxide [16]. All of the oxide powders were made by mixing appropriate amounts of $La(NO_3)_3$, $SrCO_3$, $Co(NO_3)_2 \cdot 6H_2O$, and $Fe_2O_3$ and then grinding the mixture in isopropanol with $ZrO_2$ media for 15 h. After drying, the mixtures were calcined in air at 850°C for 16 h with intermittent grinding. After final calcination, the powders were ground with an agate mortar and pestle to an average particle size of ≈7 μm. The resulting powders were characterized by X-ray diffraction (XRD), scanning electron microscopy, and thermogravimetric analysis (TGA), and analyzed for particle-size distribution.

The powder was made into a slip that contained a solvent, dispersant, binder, and plasticizer. Membrane tubes were fabricated by extruding the slip to an outside diameter of ≈6.5 mm, lengths up to ≈30 cm, and wall thicknesses of 0.25-1.20 mm. The tubes were sintered at ≈1200°C for 5-10 h in stagnant air.

Table 1. Mixed-oxide designations

| Designation | Formula |
|---|---|
| SFC-1 | $La_{0.2}Sr_{0.8}Fe_{0.6}Co_{0.4}O_x$ |
| SFC-2 | $SrFeCo_{0.5}O_x$ |
| SFC-3 | $Sr_7Fe_{6.5}Co_{3.5}O_x$ |
| SFC-4 | $Sr_2Fe_3O_x$ |
| SFC-5 | $Sr_7Fe_{10}O_x$ |
| SFC-6 | $Sr_2Fe_{3.1}O_x$ |
| SFC-7 | $SrFe_{1.2}Co_{0.5}O_x$ |
| SFC-8 | $SrFe_{0.8}Co_{0.2}O_x$ |

Mechanical properties of the finished material were measured by conventional methods, i.e., bulk density was measured by the Archimedes principle; flexural strength, in a four-point bending mode; fracture toughness, by a single-edge notch method [17]; and Young's modulus, shear modulus, and Poisson ratio, by ultrasonic methods [18]. The thermal expansion coefficient was measured with a dilatometer.

The ceramic materials were evaluated for performance in a quartz reactor system, shown in Fig. 1. The reactor supports the ceramic membrane tube with Pyrex hot seals, a design that creates an isothermal environment for the ceramic tube. To facilitate reactions and equilibration of gases in the reactor, an Rh-based reforming catalyst is loaded adjacent to the tube. Gold wire mesh is wrapped around the tube to prevent solid-state reactions between the catalyst and the ceramic. Feed gas and effluents were analyzed by gas chromotography.

Samples were prepared for conductivity and diffusional measurements by compressing the constituent powders at $1.2 \times 10^3$ MPa into pellets 21.5 mm in diameter and ≈3 mm thick. Pellets were sintered in air at ≈1200°C for 5 h; they were then cut into small bars. The bulk densities of samples were ≈95% of their theoretical values.

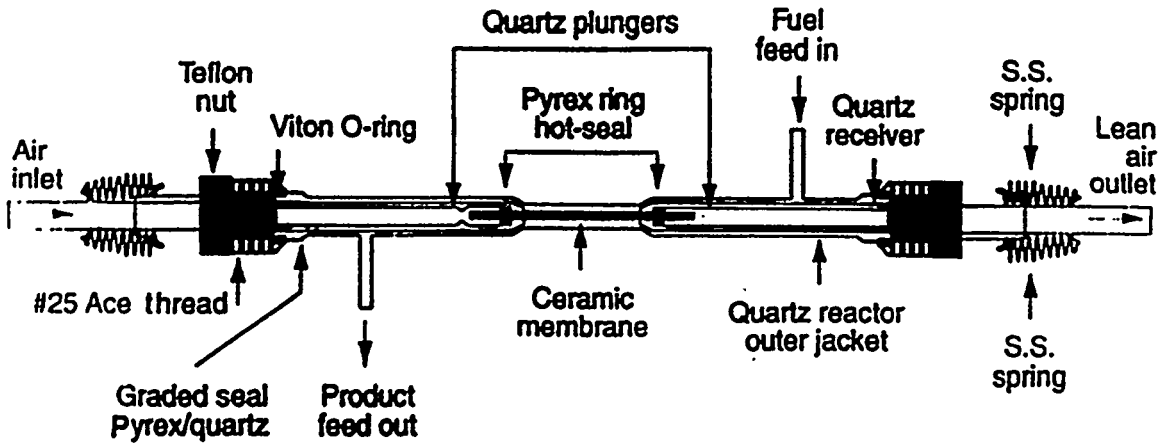


Fig. 1. Schematic diagram of ceramic membrane reactor.

Platinum wires were used as probes in the four-probe conductivity measurement. Specimen resistance was measured with an HP 4192A LF impedance analyzer. For measurement of oxygen ion conduction, yttria-stabilized zirconia (YSZ, with 8 mol% $Y_2O_3$) was used for the electron (hole) blocking electrode [19].

The oxygen diffusion coefficient was measured by a relaxation method. The sample was subjected to a sudden change in oxygen partial pressure, and ionic conductivity was then monitored as a function of time and temperature [20].

## RESULTS AND DISCUSSION

SFC-1 tubes survived only a few minutes when operated as a conversion reactor at 850°C; they then broke into several pieces. XRD patterns of the original SFC-1 samples were recorded at 850°C in Ar-$O_2$ gas mixtures. The phase behavior of SFC-1 in 1 and 20% $O_2$ is shown in Fig. 2. In an oxygen-rich atmosphere (20% $O_2$), the material was a cubic perovskite. However, once the oxygen partial pressure dropped below 5%, the cubic phase transformed to an oxygen-vacancy-ordered phase. New peaks appeared in the XRD pattern, as seen in Fig. 2 (1% $O_2$). It is important to note that this material expanded substantially after the phase transition, as can be seen from the change in the position of the Bragg peak near 32° in Fig. 2. Evidently, this peak in the oxygen-vacancy-ordered phase (in 1% $O_2$) shifted to the low-angle (larger d-spacing) side of the corresponding peak in the cubic perovskite phase (in 20% $O_2$).

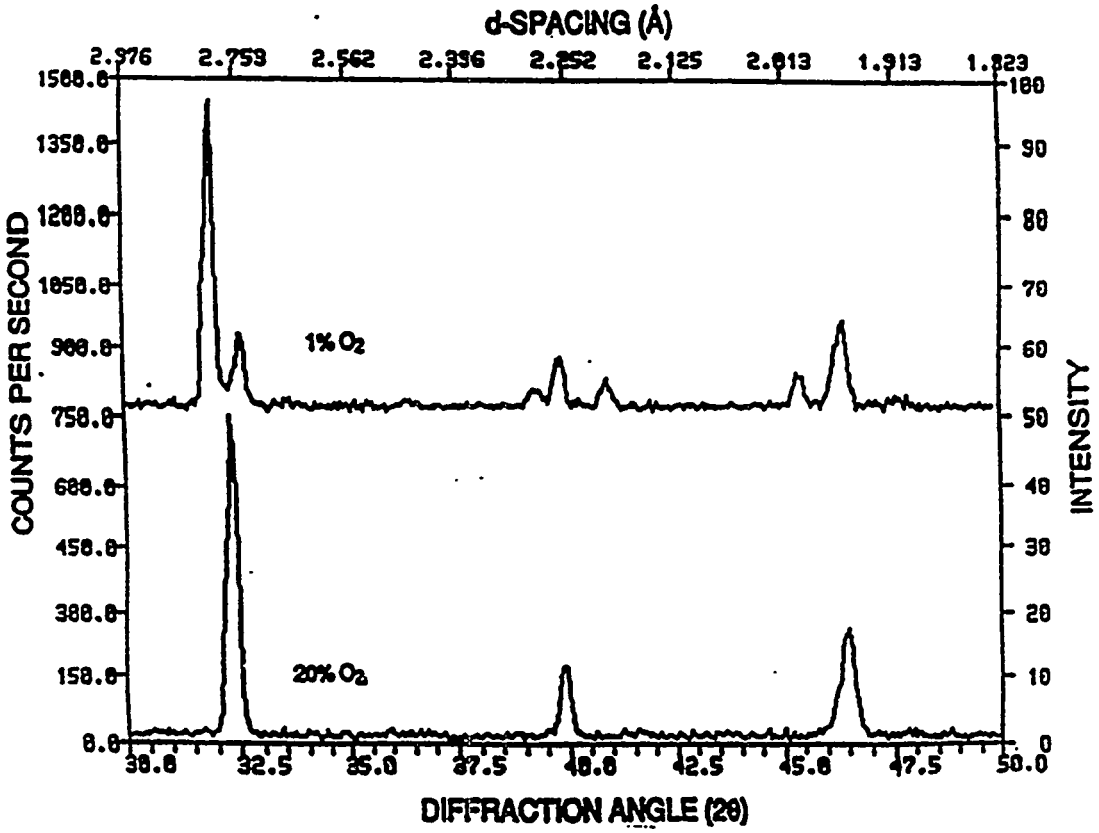


Fig. 2. XRD of SFC-1 at 850°C in 1% and 20% $O_2$ (balance is Ar).

Detailed TGA [21] showed that the oxygen content x of the SFC-1 sample in 1% $O_2$ was ≈0.1 lower than that in a sample in 20% $O_2$. Dependence of the unit cell volume on the oxygen content of the sample has been established by comparing lattice parameters. For example, the volume of the primitive perovskite cell $V_p$ is 57.51 Å$^3$ for x = 2.67 and 59.70 Å$^3$ for x = 2.48. These results show that this material expands as oxygen is removed. Such behavior suggests that an electronic effect is predominant in influencing the specific volume; otherwise, a simple size effect would cause the lattice to shrink. By linear interpolation of the above results, we predict that a decrease in x of 0.1 will result in an increase of ≈2% in $V_p$.

Both XRD and TGA data [21] give a clear picture of the state of SCF-1 under reaction conditions. When the membrane tube is in use, high oxygen pressure is maintained outside the tube and low oxygen pressure is maintained inside the tube. Before the tube is brought to high temperature, oxygen distribution is uniform.

Upon heating, the tube material begins to lose oxygen that was incorporated during the fabrication process. Moreover, the material on the

inner wall loses more oxygen than that on the outer wall. As a result, a stable oxygen gradient is generated between the outer and inner walls. It follows that the material, depending on its location in the tube, may contain different phase constituents. It is probable that the inner zone, with less oxygen, contains more ordered oxygen vacancies and hence is less oxygen-permeable.

The most remarkable factor, and one that can cause tube fracture, appears to be lattice mismatch between the materials on the inner and outer walls of the tube. The difference in composition between the inner and outer zones leads to an expansion of 2%, which is equivalent to thermal expansion caused by a 333°C temperature increase.

In comparison, SFC-2 exhibited remarkable structural stability at high temperature, as shown in Fig. 3. No phase transition was observed in this material as oxygen partial pressure was changed. Furthermore, the Bragg peaks stayed at the same position regardless of the oxygen partial pressure of the atmosphere. This structural stability of SFC-2, when compared with that of other mixed oxides, is reflected in its physical and mechanical properties, as shown in Table 2.

In all cases, SFC-2 shows above-average strength, especially in fracture toughness, which is the ability of a material to resist crack propagation.

Figure 4 shows the probability of failure vs. flexural strength (Weibull statistics) for SFC-2 [22]. The Weibull modulus was 15, indicating only moderate scatter in the strength data. Measured room-temperature properties were used to develop failure criteria for the membranes under actual reaction conditions in a plant where methane is expected to be at higher pressures. Figure 5 shows the computed allowable external pressure on SFC-2 as a function of tube wall thickness. These calculations were based on assumptions that the tensile strength is ≈0.67 times the flexural stress and that the compressive strength of SFC-2 is greater than its tensile strength by a factor of 8. These results suggest that this ceramic material can withstand reasonable stresses that might occur in a commercial reactor. Tubes made of this material, unlike those made of SFC-1, are not expected to fracture under reactor conditions.

Differences between SFC-2 and SFC-8 are observed in their electronic and ionic conductivities (Table 3) relative to those of other materials of this same type (19, 23-27). It is clear that SFC-2 is unique in that its ratio of ionic to electronic conductivity is close to unity.

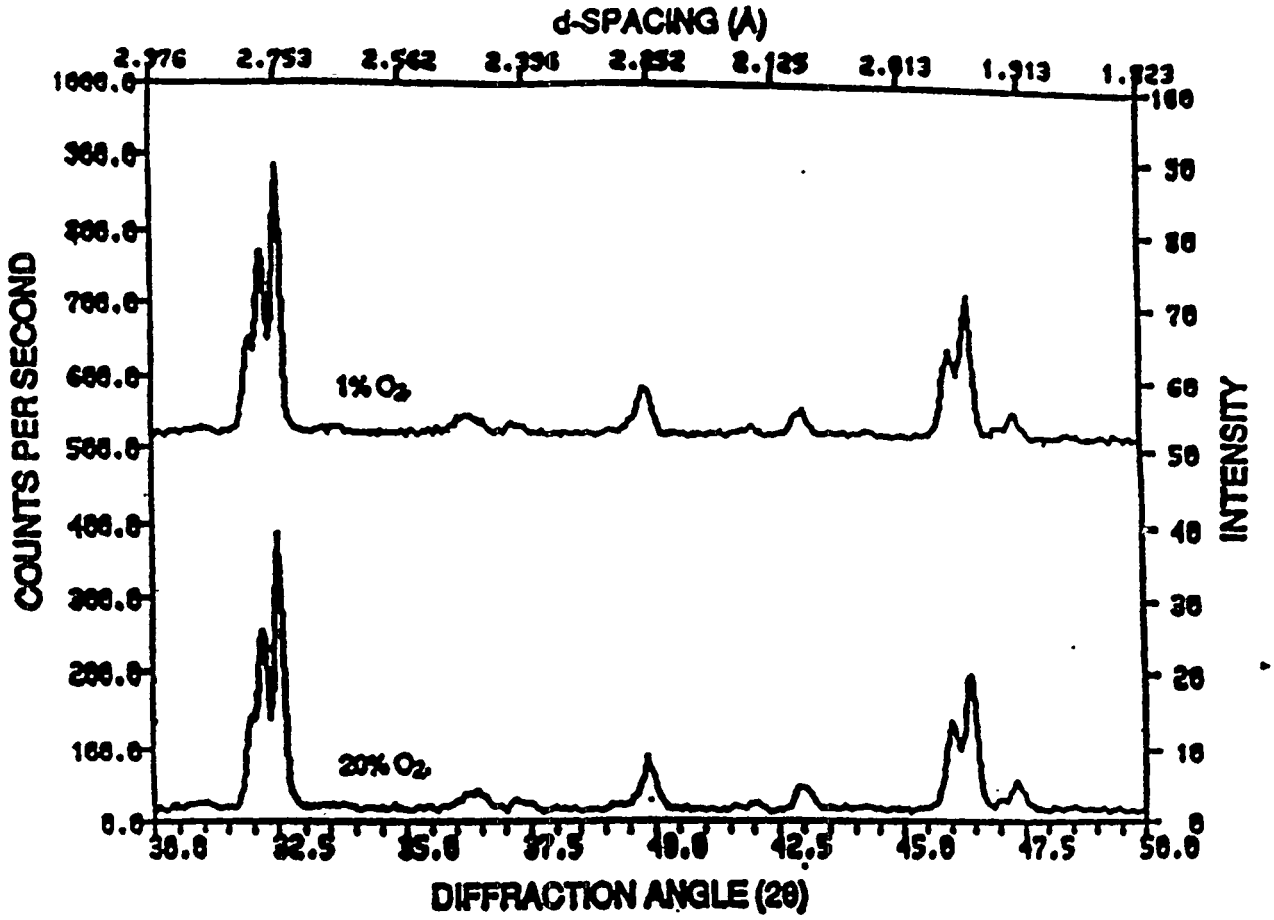


Fig. 3. XRD of SFC–2 at 850°C in 1% and 20% $O_2$ (balance is Ar).

Table 2. Physical and mechanical properties of ceramic membrane material

| Property | $SrFeCo_{0.5}O_x$ (SFC-2) | $SrFe_{1.2}Co_{0.5}O_x$ (SFC-7) | $Sr_2Fe_3O_x$ (SFC-4) | $Sr_7Fe_{10}O_x$ (SFC-5) | $Sr_2Fe_{3.1}O_x$ (SFC-6) | $Sr_7Fe_{6.5}Co_{3.5}O_x$ (SFC-3) |
|---|---|---|---|---|---|---|
| Percent of theoretical density | 93 | 97 | 87 | 80 | 94 | 92 |
| Flexural strength, MPa | 81 ± 16 | 65 ± 35 | 80 ± 20 | 78 ± 27 | 83 ± 11 | 89 ± 16 |
| Fracture toughness, $MPa\sqrt{m}$ | 2.04 ± 0.06 | 1.68 ± 0.09 | 1.02 ± 0.05 | 1.10 ± 0.08 | 1.33 ± 0.13 | 1.42 ± 0.04 |
| Young's modulus, GPa | 124 ± 3 | 85 ± 4 | 110 ± 2 | 99 ± 2 | 134 ± 52 | 120 ± 1 |
| Shear modulus, GPa | 48 ± 1 | 35 ± 1 | 43 ± 1 | 39 ± 1 | 52 ± 1 | 47 ±1 |
| Poisson ratio | 0.30 | 0.20 | 0.27 | 0.28 | 0.29 | 0.28 |

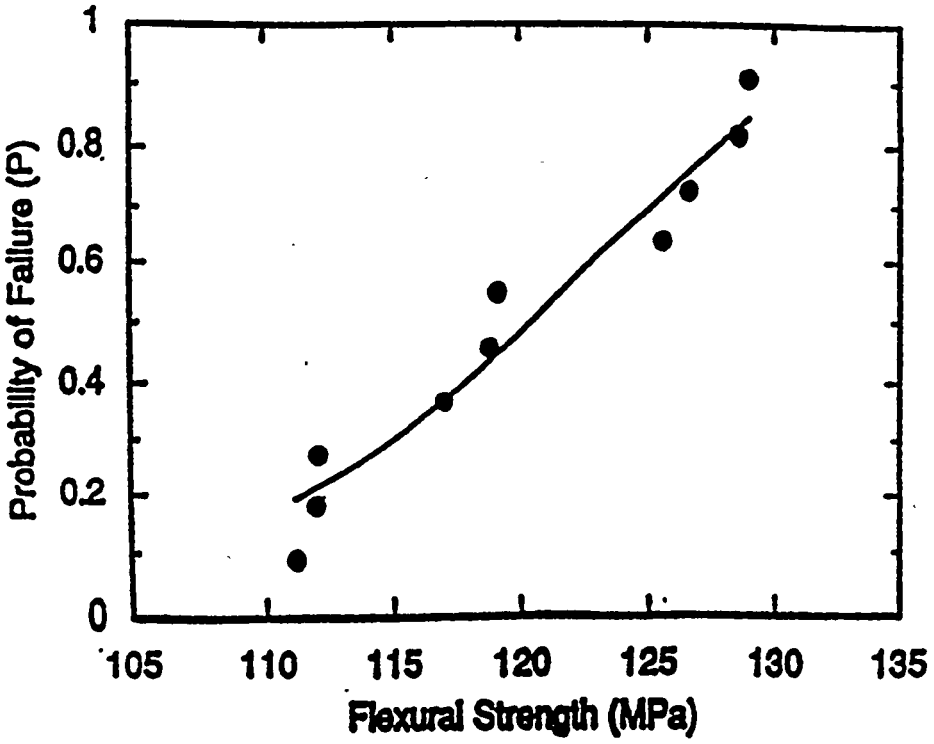


Fig. 4. Probability of failure vs. flexural strength for SFC–2 (Weibull modulus = 14.5).

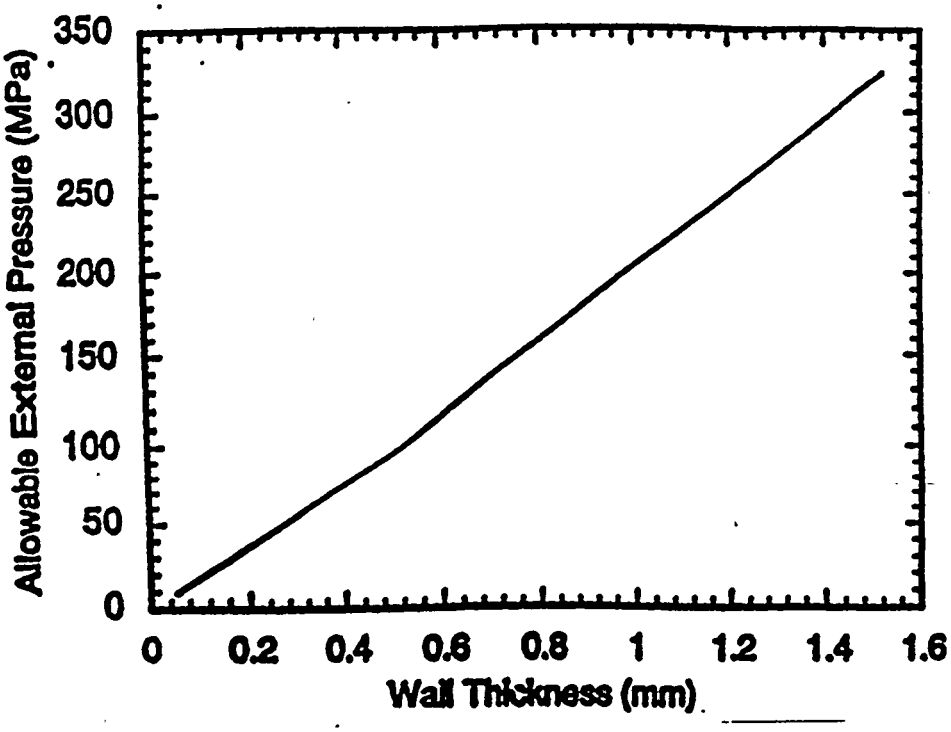


Fig. 5. Allowable external pressure on SFC–2 tubes as a function of wall thickness (O.D. = 6.40 mm).

Table 3. Conductivities of (La,Sr)(Fe,Co)$O_X$ systems, measured in air at 800°C

| Sample | Electronic $\sigma_{el}$ ($S \cdot cm^{-1}$) | Ionic $\sigma_i$ ($S \cdot cm^{-1}$) | Method for Measuring $\sigma_i$ | Ref. |
|---|---|---|---|---|
| SFC-2 | 10 | 7 | 4-terminal, YSZ electron block | 19 |
| SFC-8 | 76 | 4 | 4-terminal, YSZ electron block | 19 |
| $La_{0.6}Sr_{0.4}Co_{0.2}Fe_{0.8}O_3$ | 300 | 0.01 | 4-terminal, YSZ electron block | 23 |
| $La_{0.6}Sr_{0.4}Co_{0.2}Fe_{0.8}O_3$ | 300 | 0.003 | 2-terminal, electron block | 24 |
| $La_{0.8}Sr_{0.2}Co_{0.8}Fe_{0.2}O_3$ | 600 | 15 | 4-terminal, YSZ electron block | 25 |
| $La_{0.8}Sr_{0.2}Co_{0.8}Fe_{0.2}O_3$ | 250 | 0.10 | 4-terminal, YSZ electron block | 26 |
| $La_{0.75}Sr_{0.25}FeO_3$ | 50 | 0.03 | $^{18}O/^{16}O$ exchange | 27 |

Furthermore, limited SFC-2 diffusion data, obtained from the time-relaxation method [20], indicate that transport of oxygen ions is associated with an activation energy of 0.89 eV. This finding is consistent with the high diffusion coefficient of $9 \times 10^{-7}$ $cm^2$ $s^{-1}$ at 900°C.

Performance in generating syngas is demonstrated in Fig. 6, which shows conversion data obtained with an SFC-2 membrane tube at 850°C for ≈70 h. As shown, methane conversion efficiency is >98%, and CO selectivity is 90%. Measured $H_2$ yield is approximately twice that of CO, as expected.

The role of the catalyst in the transport of oxygen across the membrane of an SFC-2 tube was tested without the reforming catalyst. The results from a run of ≈350 h are shown in Fig. 7. The feed gases are the same as before. In the absence of a catalyst, the oxygen that was transported through the membrane reacted with methane and formed $CO_2$ and $H_2O$. As seen in Fig. 8, methane conversion efficiency was ≈35% and $CO_2$ selectivity was ≈90%. Under our operating conditions, measured oxygen flux was ≈0.3 std $cm^3/cm^2/min$. Figure 8 shows the result of a reactor run made under more severe conditions and in the presence of a catalyst for >500 h. Conversion

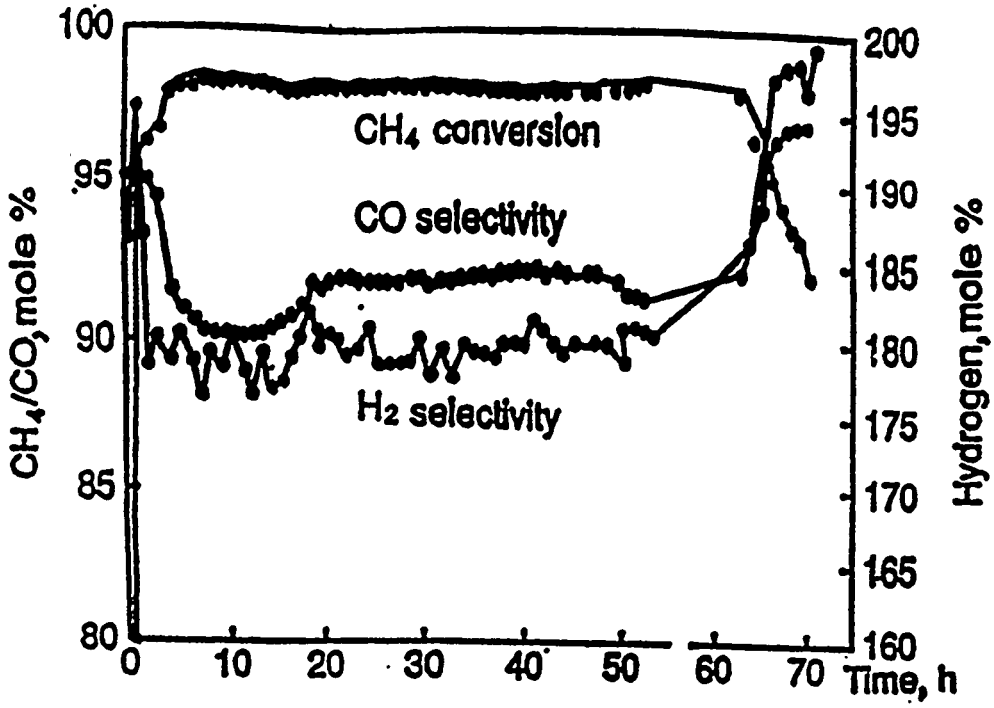


Fig. 6. Methane conversion and CO and $H_2$ selectivities in SFC–2 membrane reactor with reforming catalyst. Conditions: feed, 80% $CH_4$, 20% Ar; flow, 2.5 $cm^3$/min; temp., 850°C; pressure 1 atm; membrane surface area, 10 $cm^2$.

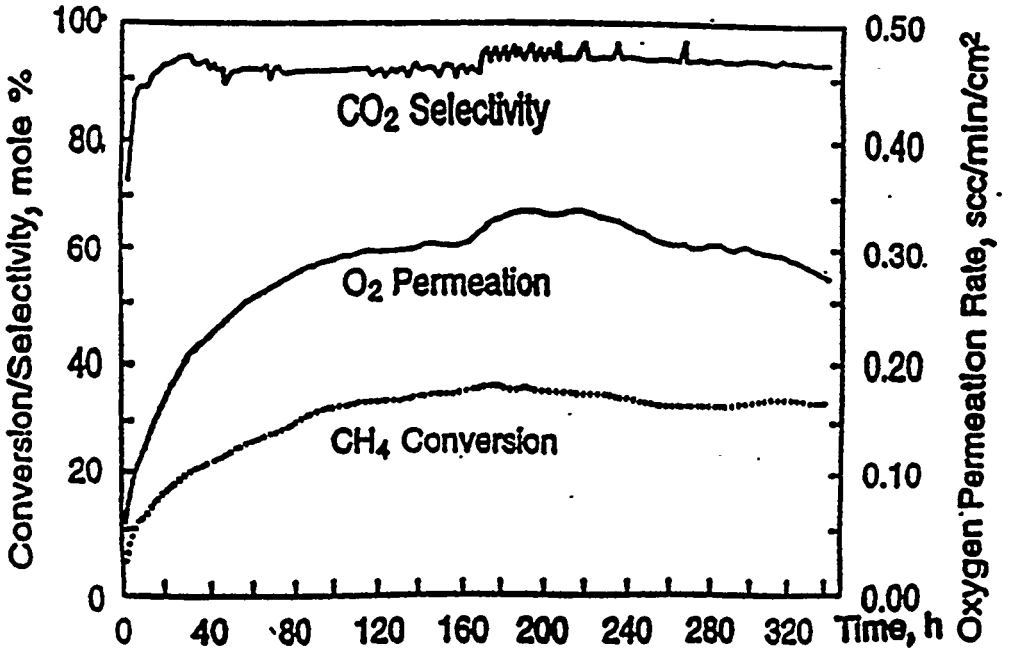


Fig. 7. Methane conversion and $CO_2$ selectivity and $O_2$ permeation in SFC-2 membrane reactor without reforming catalyst. Conditions: same as in Fig. 6.

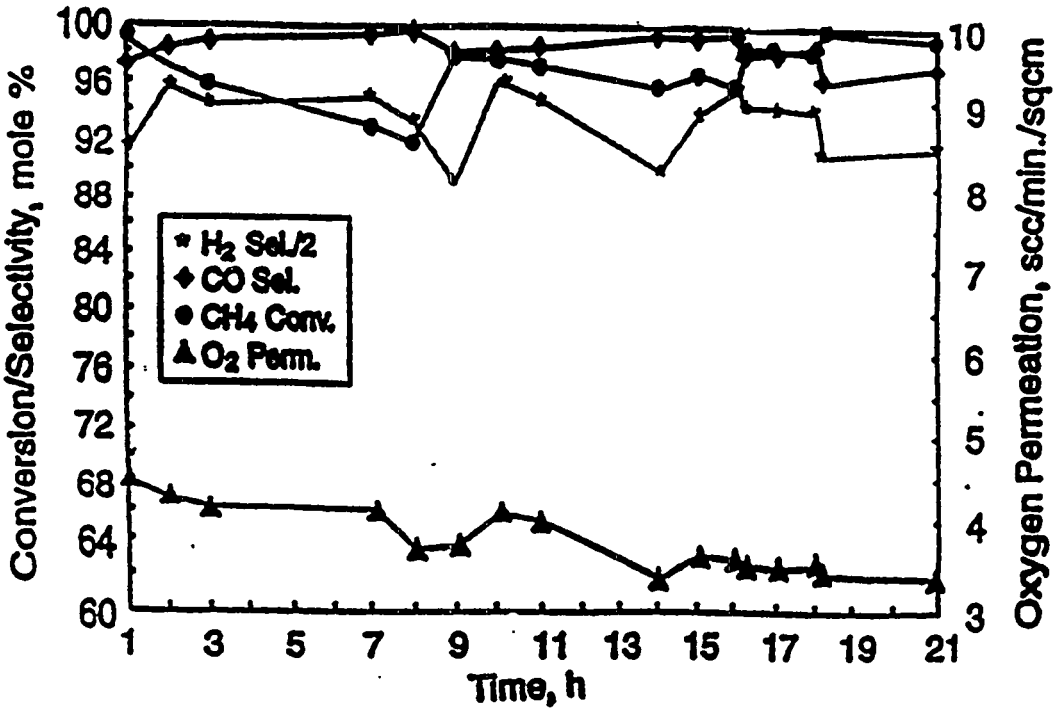


Fig. 8. Methane conversion and CO and $H_2$ selectivities and $O_2$ permeation in SFC–2 membrane reactor with reforming catalyst. Conditions: feed, 80% $CH_4$, 20% Ar; flow, 20 $cm^3$/min; temp., 900°C; pressure 1 atm; membrane surface area, 8 $cm^2$.

and selectivities are similar to those of the 350–h run but the oxygen flux was one order of magnitude greater. Some small deactivation in oxygen permeation rate was observed.

Further confirmation of the stability of this membrane tube is shown in Fig. 9, which shows reactor results over a period of 1000 h. The feed during this period was a typical mixture expected in a commercial recycling feed, namely methane, CO, $CO_2$, and $H_2$. Throughout the run, methane conversion was high. A small decline in oxygen permeation was observed. However, this high oxygen flux is consistent with the high diffusion coefficient of 9 x $10^{-7}$ $cm^2$ $s^{-1}$ that was measured by the time–relaxation method [20].

A further run of 1000 h, seen in Fig. 10, was made with a methane/argon feed. During this run, the temperature was changed several times. To compensate for the resulting change in reaction rate, the feed

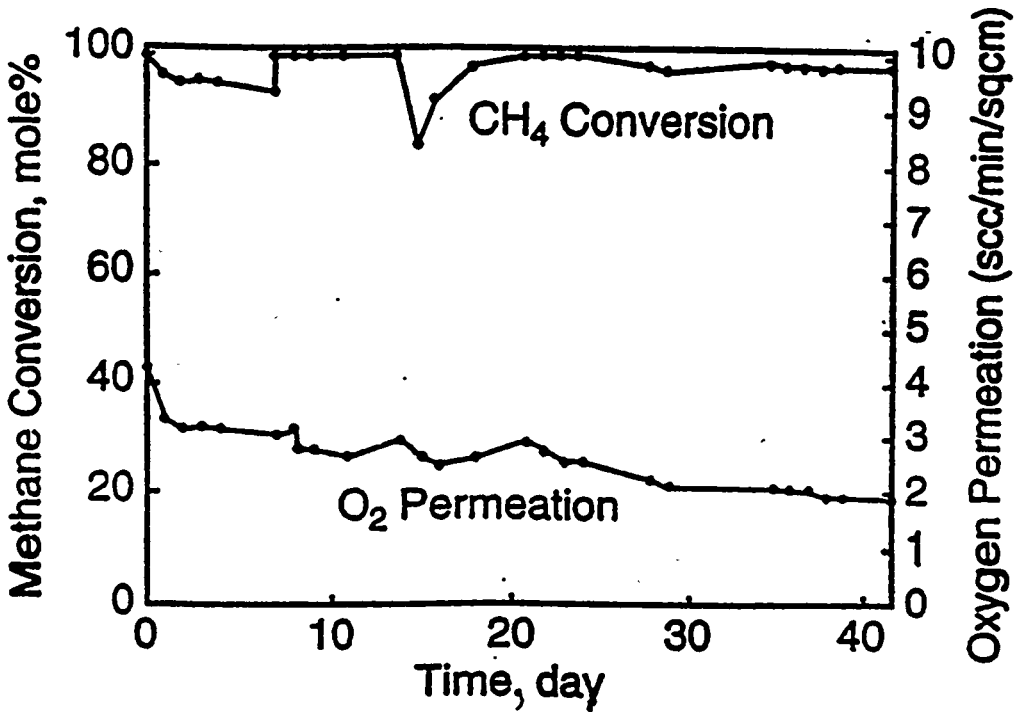


Fig. 9. Methane conversion and $O_2$ flux for a mixed feed. Conditions: feed, 80% $CH_4$, 20% Ar; temp., 900°C; pressure 1 atm; catalyst, 1.5 g; membrane surface area, 8.4 $cm^2$.

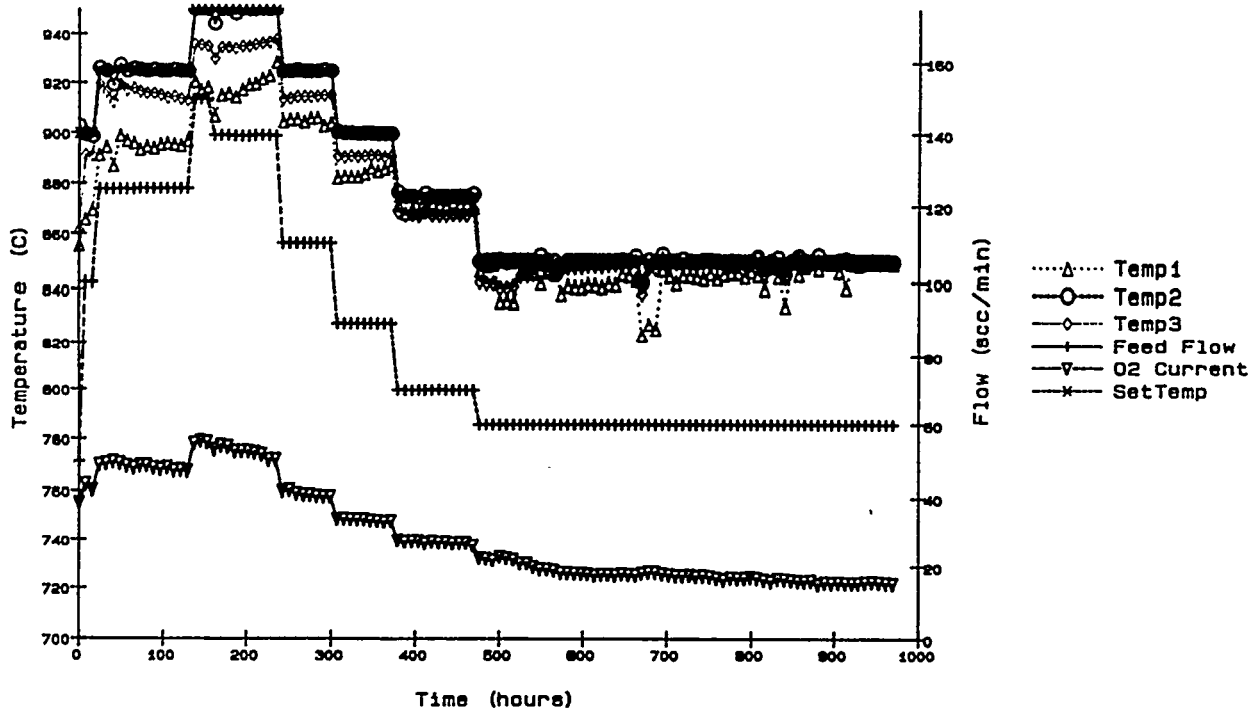


Air=1.2 l/m, Pres=~1atm, Membrane SA=4.4sqcm, Wall=.75mm, Cat=2.5g

Fig. 10. Temperature profile and $O_2$ current in membrane.

flow rate was altered accordingly. The selectivity to CO during the entire run remained >98%. Oxygen permeability followed the changes in temperature and feed flow.

Application of the oxygen permeability data obtained from simple geometry such as tubes to large-scale reactor configurations requires an oxygen transport model across the ceramic membrane. Recently, an oxygen transport equation was developed [28] on the basis of the phenomenological theory of diffusion to describe the effects of temperature, membrane thickness, and driving force on oxygen flux. It is shown that the oxygen permeability observed in reactor experiments can be adequately described by

$$J_{O^{2-}} = \frac{1}{2}\frac{D_{eff}c_{O^{2-}}}{L}\ln\left(\frac{p^{I}_{O_2}}{p^{II}_{O_2}}\right)$$

where $J_{O^{2-}}$ is the oxygen flux across a thin wall tube of wall thickness, $D_{eff}$ is the effective diffusion coefficient of oxygen in species, $c_{O^{2-}}$ is the concentration of oxygen ions in the material, and $p^{I}_{O_2}$ and $p^{II}_{O_2}$ are the oxygen partial pressures on the air and methane side, respectively.

Thermodynamic calculations were made [28] to calculate the oxygen partial pressure on the methane side, assuming that all of the oxygen transported through the tube is consumed in the conversion of methane to syngas. The permeablity data obtained from the reactor in combination with the model (see Fig. 11) yielded

$$D_{eff} = 4.37 \exp\left(\frac{-156{,}000}{RT}\right) \text{cm}^2/\text{s}.$$

where the activation energy of 156 kJ/mole is within the range of values reported [29] for La-based nonstoichiometric perovskite structure oxides. The experimentally observed results of the oxygen flux agree within 25% of the predicted, as seen in Fig. 12.

## CONCLUSIONS

Mixed-conducting ceramic materials have been produced from mixed-oxide systems of the La-Sr-Fe-Co-O (SFC) type, in the form of tubes and bars. Thermodynamic stability of the tubes was studied as a function of oxygen partial pressure by high-temperature XRD. Mechanical properties of

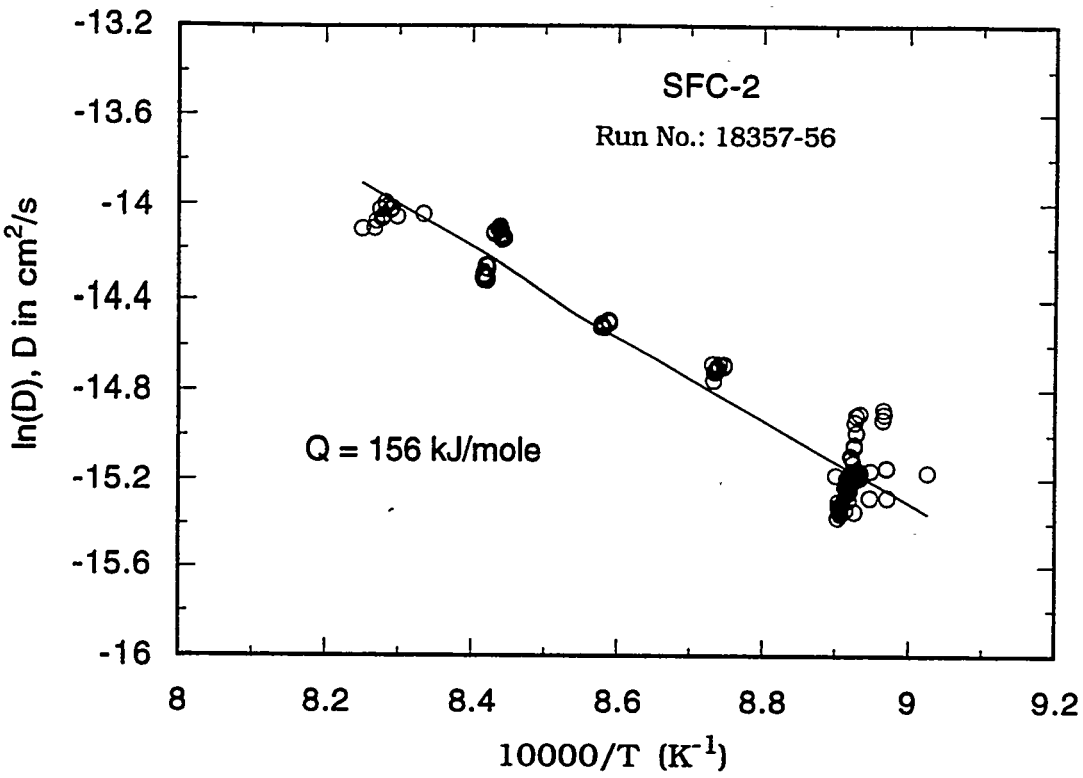


Fig. 11. Temperature dependence of $O_2$ diffusivity in SFC–2.

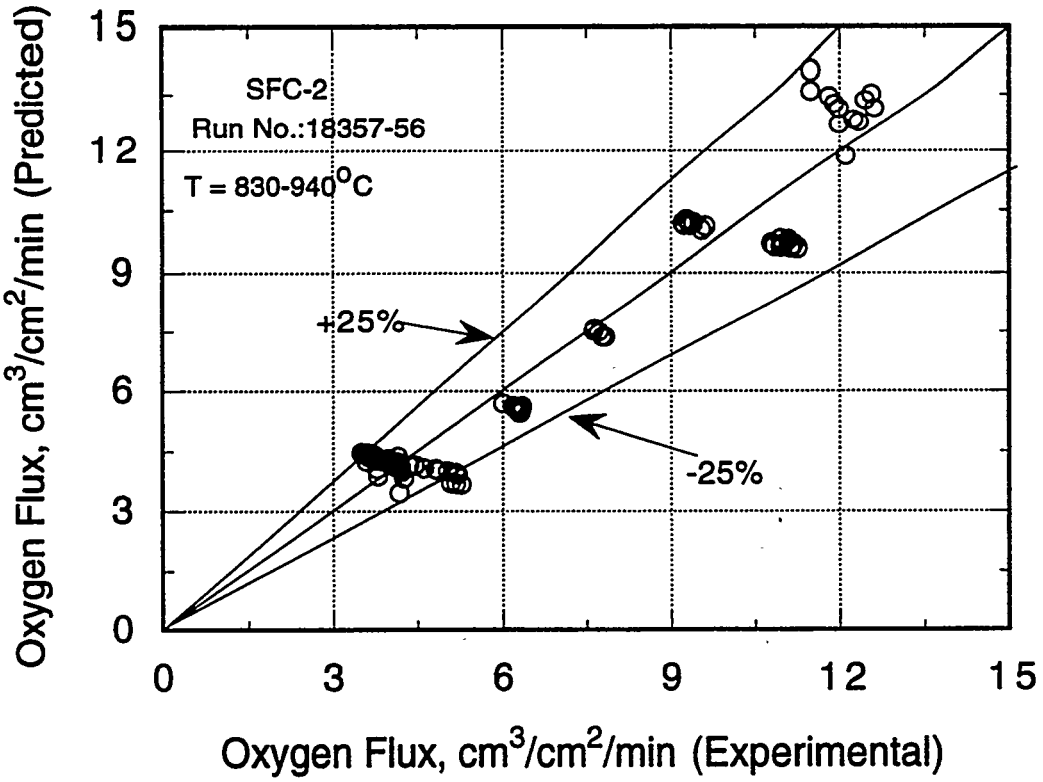


Fig. 12. Predicted $O_2$ flux vs. experimentally determined $O_2$ flux.

the SFC–2 material were adequate for reactor use. Electronic and ionic conductivities showed that SFC–2 is unique in that its ratio of ionic to electronic conductance is close to unity.

Performance of the membrane tubes was good only with SFC–2. Fracture of other SFC tubes was the consequence of an oxygen gradient that introduced a volumetric lattice difference between the inner and outer walls. SFC–2 tubes provided methane conversion efficiencies >99% in a reactor and have operated successfully for >1000 h.

## ACKNOWLEDGMENTS

Work at Argonne National Laboratory is supported by the U.S. Department of Energy, Pittsburgh Energy Technology Center, under Contract W-31-109-Eng-38.

## REFERENCES

1. Y. Teraoka, H. M. Zhang, S. Furukawa, and N. Yamozoe, *Chem. Lett.*, **1985**, 1743, 1985.

2. Y. Teraoka, T. Nobunaga, and N. Yamazoe, *Chem. Lett.*, 503, 1988.

3. T. J. Mazanec, T. L. Cable, and J. G. Jr. Frye, *Solid State Ionics*, 53, 1992.

4. A. C. Bose, J. G. Stigel, and R. D. Srivastava, "Gas to Liquids Research Program of the U.S. Department of Energy: Programmatic Overview," paper presented at *Symp. on Alternative Routes for the Production of Fuels*, American Chemical Society National Meeting, Washington, DC, Aug. 21-26, 1994.

5. U. Balachandran, S. L. Morissette, J. T. Dusek, R. L. Mieville, R. B. Poeppel, M. S. Kleefisch, S. Pei, T. P. Kobylinski, and C. A. Udovich, in *Proc. Coal Liquefaction and Gas Conversion Contractors Rev. Conf.* (S. Rogers et al., eds.), Vol. 1, pp. 138-160, U.S. Department of Energy, Pittsburgh Energy Technology Center, Pittsburgh, PA, Sept. 27-29, 1993.

6. T. L. Cable, European Patent EP 0438 902 A2, July 31, 1991.

7. E. A. Hazbun, U.S. Patent 4,791,079, Dec. 13, 1988.

8. K. Omata, S. Hashimoto, H. Tominaga, and K. Fujimoto, *Appl. Catal.*, **52** (1989) L1.

9. U. Balachandran, S. L. Morissette, J. J. Picciolo, J. T. Dusek, R. B. Poeppel, S. Pei, M. S. Kleefisch, R. L. Mieville, T. P. Kobylinski, and C. A. Udovich, in *Proc. Int. Gas Res. Conf.* (H. A. Thompson, ed.) pp. 565-573, Government Institutes, Inc., Rockville, MD, 1992.

10. T. M. Gur, A. Belzner, and R. A. Huggins, J. Membrane Sci., **75**, 151, 1992.

11. T. L. Cable, European Patent EP 0 399 833 Al, Nov. 28, 1990.

12. R. D. Evans, An Introduction to Crystal Chemistry, Cambridge University Press, Cambridge, England, 1964.

13. N. G. Eror and U. Balachandran, *J. Solid State Chem.* **40**, 85, 1981.

14. U. Balachandran and N. G. Eror, *J. Phys. Chem. Solids*, **44**, 231, 1983.

15. N. G. Eror and U. Balachandran, *J. Amer. Ceram. Soc.*, **65**, 426, 1982.

16. U. Balachandran, M. Kleefisch, T. P. Kobylinski, S. L. Morissette, and S. Pei, International Patent WO94/24065, Oct. 1994.

17. W. F. Brown, Jr. and J. E. Strawley, ASTM STP 410, Philadelphia, PA, 1967.

18. J. Kraütkramer and H. Kraütkramer, Ultrasonic Testing of Materials (Springer–Verlag, New York, 1983).

19. B. Ma, J.–H. Park, U. Balachandran, and C. U. Segre, "Electronic/Ionic Conductivity and Oxygen Diffusion Coefficient of the Sr–Fe–Co–O System," Materials Research Society Spring Meeting, San Francisco, CA, April 17–21, 1995.

20. B. Ma, U. Balachandran, J.–H. Park, and C. U. Segre, submitted to *Solid State Ionics.*, 1995.

21. S. Pei, M. S. Kleefisch, T. P. Kobylinski, J. Faber, C. A. Udovich, V. Zhang–McCoy, B. Dabrowski, U. Balachandran, R. L. Mieville, and R. B. Poeppel, *Catal. Lett/*, **30**, 201, 1995.

22. W. Weibull, *J. Appl. Mech.*, **293**, 18, 1951.

23. H. U. Anderson, C. C. Chen, L. W. Tai, and M. M. Nasrallah, in *Proc. 2nd Intl. Symp. on Ionic and Mixed Conduction Ceramics* (T. A. Ramanarayaman, W. L. Worrell, and H. L. Tuller, eds.) pp. 376-387, The Electrochem. Soc., Pennington, NJ, 1994.

24. C. C. Chen, M. M. Nasrallah, and H. U. Anderson, submitted to *J. Electrochem. Soc.*, 1994.

25. W. L. Worrell, P. Han, and J. Huang, in *High Temperature Electrochemical Behavior of Fast Ion and Mixed Conductors* (F. W. Poulsen, J. J. Bertzen, T. Jacobson, E. Skou, and M. J. L. Ostergood, eds.), Risø National Laboratory, Roskilde, Denmark, 1993) pp. 461-466.

26. Y. Teraoka, H. M. Zhang, K. Okamoto, and N. Yamazoe, *Mater. Res. Bull.*, **23**, 51, 1988.

27. T. Ishigaki, S. Yamauchi, K. Kishio, J. Mizusaki, and K. Fuek, *Solid State Chem.*, **73**, 179, 1988.

28. P. S. Maiya, M. S. Kleefisch, J. T. Dusek, R. L. Mieville, U. Balachandran, and C. A. Udovich, paper for presentation at the 1st Intl. Conf. on Ceramic Membranes, 188th Mtg. of the Electrochem. Soc., Inc., Chicago, IL, October 8–13, 1995.

29. S. Carter, A. Selcuk, R. J. Chater, K. Kajda, J. A. Kilner, and B. C. H. Steele, *Solid State Ionics*, **53–56**, 597, 1992.